JNCI J Natl Cancer Inst (2016) 108(3): djv330

doi:10.1093/jnci/djv330
First published online November 22, 2015
Article

ARTICLE

Restoring Anticancer Immune Response by Targeting Tumor-Derived Exosomes With a HSP70 Peptide Aptamer

Jessica Gobbo, Guillaume Marcion, Marine Cordonnier, Alexandre M. M. Dias, Nicolas Pernet, Arlette Hammann, Sarah Richaud, Hajare Mjahed, Nicolas Isambert, Victor Clausse, Cédric Rébé, Aurélie Bertaut, Vincent Goussot, Frédéric Lirussi, François Ghiringhelli, Aurélie de Thonel, Pierre Fumoleau, Renaud Seigneuric*, Carmen Garrido*

Affiliations of authors: INSERM, UMR 866, Laboratoire d'Excellence LipSTIC, Dijon, France (JG, GM, MC, AMMD, NP, AH, SR, HM, NI, VC, CR, FL, FG, AdT, RS, CG); Faculty of Medicine and Pharmacy, University of Burgundy, Dijon, France (JG, GM, MC, AMMD, NP, AH, SR, HM, NI, VC, CR, FL, FG, AdT, RS, CG); Department of Medical Oncology, Georges-François Leclerc Centre, Dijon, France (JG, NI, CR, AB, VG, FG, PF, CG); Department of Biostatistics, Georges-François Leclerc Centre, Dijon, France (AB); CHU, Dijon, France (FL); Equipe Labellisée par la Ligue Nationale contre le Cancer (CG).

*Authors contributed equally to this work.

Correspondence to: Carmen Garrido, PhD, INSERM UMR866, Faculty of Medicine and Pharmacy, 7 Boulevard Jeanne d'Arc, 21079 Dijon, France (e-mail: cgarrido@u-bourgogne.fr).

Abstract

Background: Exosomes, via heat shock protein 70 (HSP70) expressed in their membrane, are able to interact with the toll-like receptor 2 (TLR2) on myeloid-derived suppressive cells (MDSCs), thereby activating them.

Methods: We analyzed exosomes from mouse (C57Bl/6) and breast, lung, and ovarian cancer patient samples and cultured cancer cells with different approaches, including nanoparticle tracking analysis, biolayer interferometry, FACS, and electron microscopy. Data were analyzed with the Student's *t* and Mann-Whitney tests. All statistical tests were two-sided.

Results: We showed that the A8 peptide aptamer binds to the extracellular domain of membrane HSP70 and used the aptamer to capture HSP70 exosomes from cancer patient samples. The number of HSP70 exosomes was higher in cancer patients than in healthy donors (mean, ng/mL ± SD = 3.5 ± 1.7 vs 0.17 ± 0.11, respectively, $P = .004$). Accordingly, all cancer cell lines examined abundantly released HSP70 exosomes, whereas "normal" cells did not. HSP70 had higher affinity for A8 than for TLR2; thus, A8 blocked HSP70/TLR2 association and the ability of tumor-derived exosomes to activate MDSCs. Treatment of tumor-bearing C57Bl/6 mice with A8 induced a decrease in the number of MDSCs in the spleen and inhibited tumor progression (n = 6 mice per group). Chemotherapeutic agents such as cisplatin or 5FU increase the amount of HSP70 exosomes, favoring the activation of MDSCs and hampering the development of an antitumor immune response. In contrast, this MDSC activation was not observed if cisplatin or 5FU was combined with A8. As a result, the antitumor effect of the drugs was strongly potentiated.

Conclusions: A8 might be useful for quantifying tumor-derived exosomes and for cancer therapy through MDSC inhibition.

Received: March 28, 2015; **Revised:** June 23, 2015; **Accepted:** October 12, 2015

A growing body of evidence suggests that the success of an anticancer therapy depends on anticancer immune response efficiency (1,2). Recent studies identified myeloid cells as potent suppressors of tumor immunity and therefore represent a major limitation for cancer immunotherapy (3). These myeloid-derived suppressor cells (MDSCs) accumulate in the blood, spleen, lymph nodes, bone marrow, and at tumor sites in most patients and in experimental models. MDSCs play a major role in the inhibition of both adaptive and innate immunity (4). MDSCs are considered essential actors in the immune dysfunction observed in most patients with sizable tumor burdens (5). Accordingly, the presence of MDSCs in cancer patients is associated with poor survival and tumor progression (6,7). How MDSCs affect the immune system remains unclear but they likely act via the suppression of lymphocytes and natural killer (NK) cell activity.

Exosomes are nanovesicles (diameter: ~50–200 nm) released into the extracellular environment via the endosomal vesicle pathway by fusion with the plasma membrane (8,9). A broad range of cells secrete exosomes, including T/B, epithelial, dendritic, and tumor cells (10–13). Exosomes are essential for intercellular communication (14). Tumor-derived exosomes (TDEs) have been reported to play a major role in the formation of primary tumors and metastases (15) and in modulating antitumor immune responses (16). Chalmin et al. have recently demonstrated that TDEs, through membrane-anchored HSP70, can activate MDSCs (17). Indeed, MDSC activation results from the interaction between toll-like receptor 2 (TLR2) and HSP70 on the exosomes. This interaction leads to the stimulation of the nuclear factor–kappa B signaling pathway and then activation of the signaling pathway JAK2 (Janus Kinase)/STAT3 through IL-6 autocrine secretion. HSP70 is a stress-inducible heat shock protein with intra- and extracellular (danger signal) functions. Intracellular roles of HSP70 include the chaperone function through the stabilization of protein 3D structures, prevention of unfolded protein aggregation, and anti-apoptotic functions (18,19). HSP70 is overexpressed in many cancer cells and confers resistance to chemotherapeutic drugs, promoting cancer development. Because of its overexpression, HSP70 can be found at the plasma membrane of cancer cells but not normal cells (20–22).

We previously selected peptide aptamers (either of 8 or 13 amino acids inserted into *E. coli* thioredoxin scaffold) that were able to bind different regions of HSP70 (23) through their unique doubly constrained target-binding loop (24,25). We demonstrated that one of them, A8, inhibits HSP70 chaperone activity and displays strong anticancer properties in syngeneic mouse models but not in nude mice (23).

Methods

Cells and Products

B16F10 (mouse melanoma), CT26 (mouse colon cancer), HCT116 (human colon cancer), SW480 (human colon cancer), PC3 (human prostate cancer), HeLa (human cervix cancer) EL4 (mouse lymphoma) cell lines (American Type Culture Collection [ATCC]) were cultured in RPMI 10% foetal bovine serum (FBS; Lonza); mouse embryonic fibroblasts (MEF) were cultured in DMEM 10% FBS (Lonza). Further details are given in the Supplementary Methods (available online).

Mouse Experiments

Wild-type C57Bl/6 mice were purchased from Charles River, France. The mice were between eight and 10 weeks old (max 10 mice per cage) were housed at the central animal facility (Dijon, France). The mice were fed with A04-10 diet (Safe Augy, France) and tap water was provided ad libitum through an automatic watering system (Edstrom Europe, Hereford, UK). All procedures were carried out in accordance with institutional policies following approval from the Animal Ethical Board of Dijon (C2EA, Grand Campus 105, n°01674.01).

Patients and Samples

Breast, pulmonary, and ovary cancer patients were informed that their urines samples might be used for research and were given the opportunity to refuse the use of their samples. This study was approved by the local ethics committee (IRB 00010311, Centre Georges-François Leclerc, Dijon).

Exosome Purification

Cells were cultured in medium depleted from serum-derived exosomes. Supernatants were collected from cell lines and sequentially centrifuged at 300 xg for 10 minutes (4°C) and at 2000 xg for 10 minutes. Then, exosomes were ultracentrifugated at 100 000 xg for 70 minutes and washed in PBS. The same protocol was used for urine and blood samples. To evaluate exosome concentrations, we used a NanoSight LM10 instrument (NanoSight, Amesbury, UK).

Biolayer Interferometry

Protein-protein interaction experiments were conducted with an Octet Red instrument (FortéBio, Menlo Park, CA). The ligand (A8 or TLR2) was biotinylated using EZ-Link NHS-PEG_4-biotin (2 nM, 30 min, RT, Thermo Fisher Scientific, Germany) and immobilized on streptavidin sensors (black 96-well plate, FortéBio). Further details are given in the Supplementary Methods (available online).

pSTAT3 Analysis

Myeloid suppressive cells 2 (MSC2) ($2x10^6$) or MDSCs ($2x10^6$) were incubated alone or with exosomes (from B16F10, CT26, HCT116, SW480) in the absence or presence of A8 or A17 (16 μM) for six hours (RPMI 10% FBS, 5% of CO_2 at 37°C). Every two hours, $5x10^6$ cells were sampled and centrifugated five minutes at 300 xg. Cells were lysed in lysis buffer (50 mM HEPES [pH 7.6], 150 mM NaCl, 5 mM EDTA, and 0.1% NP40 and antiphosphatases, Roche). Then, pSTAT3 and STAT3 expression were analyzed by western blotting.

MDSC Cell Isolation and Analysis

Single-cell suspensions were prepared from spleens, and red cells were removed using ammonium chloride lysis buffer. Gr-1+ cells were isolated from spleens of different group of tumor-bearing mice or naive mice by labeling the cells with PE-Cy7 Ab to Gr-1, then using magnetic PE-Cy7 beads and LS MACS columns (Miltenyi Biotec). For extracellular staining of immune markers, single-cell suspensions were prepared. We incubated $1x10^6$ freshly prepared cells with fluorochrome-coupled CD11b antibody (eBioscience). All events were acquired by a BD Bioscience LSR-II device and analyzed with FlowJo (Tree Star).

Lymphocyte Isolation and Coculture Experiment

Single-cell suspensions were prepared from spleens, and red cells were removed using ammonium chloride lysis buffer.

ARTICLE

Lymphocytes were isolated from spleens of naive mice in a two-step procedure. Further details are given in the Supplementary Methods (available online).

Histologic Study of the Tumor

Mice were killed 15 or 18 days after cell injection. The site of tumor cell injection was resected and snap-frozen in liquid nitrogen. An immunohistochemical study of tumor-infiltrating inflammatory cells was performed on acetone-fixed 5 µm cryostat sections. Further details are given in the Supplementary Methods (available online).

MSC2 and MDSC Cell Proliferation Analysis

MSC2s' proliferation was analyzed by two different techniques. First, MSC2s ($1x10^4$) were seeded onto 16-well plates with medium containing 10% FBS and incubated for 34 hours. Then, cells were treated or not with exosomes (from B16F10) in the absence or presence of A8 (16 µM) for five days. Further details are given in the Supplementary Methods (available online).

Tumor Growth Analysis in Vivo

B16F10 cells ($5x10^4$) or EL4 ($7x10^5$) cells were injected s.c. into the right flank of C57BL/6 mice (Charles River, France) (n = 6 per group). Tumor volumes were evaluated every two days. Mice (n = 6 per group) were treated with a control peptide aptamer A0 (3 mg/kg) or aptamer A8 (3 mg/kg) and/or cisplatin (CDDP, 5 mg/kg) or 5-fluorouracil (5FU, 25 mg/kg).

Statistical Methods

Quantitative results are expressed as means ± SD from at least three independent experiments. Quantitative data were compared using the Student's *t* test or Mann-Whitney according to their distribution. All statistical tests were two-sided, and error bars in the graphs represent standard deviations. Graphics were analyzed using the GraphPad Prism program.

Results

HSP70 Peptide Aptamer A8 Can Be Used to Capture HSP70 Exosomes From Cancer Patient Samples

We previously showed that exosomes from mouse CT26 cancer cells expressed HSP70 on their membranes (HSP70 exosomes), which was responsible for MDSC activation (17). Membrane-bound HSP70 presents an extracellular sequence composed of 14 amino acids in the C-terminal region, against which a monoclonal antibody was raised (cmHSP70) (26). We previously described the selection of an 8-amino-acid peptide aptamer A8 (23) that binds within the peptide-binding domain of HSP70 (Supplementary Figure 1, A and B, available online). To determine whether A8 could precisely associate to the extracellular sequence of membrane-bound HSP70 and therefore could be used to capture tumor-derived exosomes, we analyzed its ability to bind to extracellular HSP70 in the membrane of TDEs. Biolayer interferometry (BLI) showed that A8 efficiently captured exosomes and that it strongly decreased the ability of cmHSP70 to bind to membrane HSP70, indicating that both molecules may compete for the same extracellular epitope of HSP70 on the exosomes (Figure 1A).

We next validated this BLI protocol with urine samples from cancer patients (breast, lung, and ovary cancers, n = 8) and healthy donors (n = 5). The results found with this protocol (Figure 1B) were confirmed by customized ELISA analysis (Figure 1C). The number of HSP70 exosomes was higher in all cancer patients compared with healthy donors, for whom hardly any HSP70 exosomes could be detected, as shown in Figure 1B (mean signal = 0.07 nm ± 0.02 vs mean signal = 0.018 nm ± 0.003, $P < .001$) and Figure 1C (3.5 ng/mL ± 1.7 vs 0.17 ng/mL ± 0.11, $P = .004$). These results were highlighted by the fact that the total number of exosomes quantified by NanoSight in urine samples was in fact higher in healthy donors than in cancer patients, with mean exosome concentrations of 261 x 10^9 particles/mL ± 86 (control subjects) vs 66 x 10^9 particles/mL ± 36 (patients) ($P = .0016$) (Figure 1D; Supplementary Figure 2, available online).

HSP70 Exosomes Are Released From Tumor Cells

To study how HSP70 exosomes are specific markers of tumor-derived exosomes, we started evaluating the release of exosomes in culture media from four cancer cell lines (HCT116 and SW480 human colon cancer, CT26 mouse colon carcinoma and B16F10 mouse melanoma), in the noncancerous mouse embryonic fibroblasts (MEFs) and primary cultures of colon intestinal epithelial cells (NCMs). First, to avoid any artifact related to the presence of other microvesicles potentially copurified with exosomes, we validated the expression of specific classical markers of exosomes in all samples such as Flotillin-1 and CD81 (Figure 2A). Next, to determine the presence of HSP70 in the membranes of exosomes, we used flow cytometry (Figure 2B), standard transmission electronic microscopy (Supplementary Figure 3A, available online), and our BLI protocol to capture HSP70 exosomes (Figure 2C). All these different techniques indicated that extracellular HSP70 was detectable only at the surface of exosomes derived from the cancer cell lines analyzed. We further validated that HSP70 exosomes were a general feature of cancer cells by analyzing a broader panel of cancer cells: prostate PC3, lymphoma EL4, cervix HeLa, and breast cancer MCF-7. They were compared with the following noncancerous cells: prostate PrEC cells, primary lymphocytes (PLs), uterine cells (PUCs), and breast epithelial cells (HMECs). As shown in Figure 2D, we found that all cancer cells released a high amount of HSP70 exosomes as compared with their normal counterparts, for which hardly any release of HSP70 exosomes could be detected.

Paralleling the analysis of membrane-bound HSP70 in the exosomes, we checked the expression of HSP70 in the plasma membrane of different cells by immunofluorescence and FACS analysis (Supplementary Figure 3, B and C, and not shown). We observed that, as already reported, membrane-bound HSP70 was only detected in cancer but not in normal cells. This could explain why release of exosomes presenting HSP70 at their membranes may be a general feature of a cancer cells.

A8 Blocks the Ability of HSP70 to Associate With TLR2

Activation of MDSC by exosomes is mediated via the binding of extracellular HSP70 to TLR2 expressed on MDSC (17). We therefore studied whether A8 could interfere with HSP70/TLR2 interaction. As shown in Figure 3A, HSP70 association to TLR2 was inhibited by A8 in a dose-dependent manner (from 0.3 µM

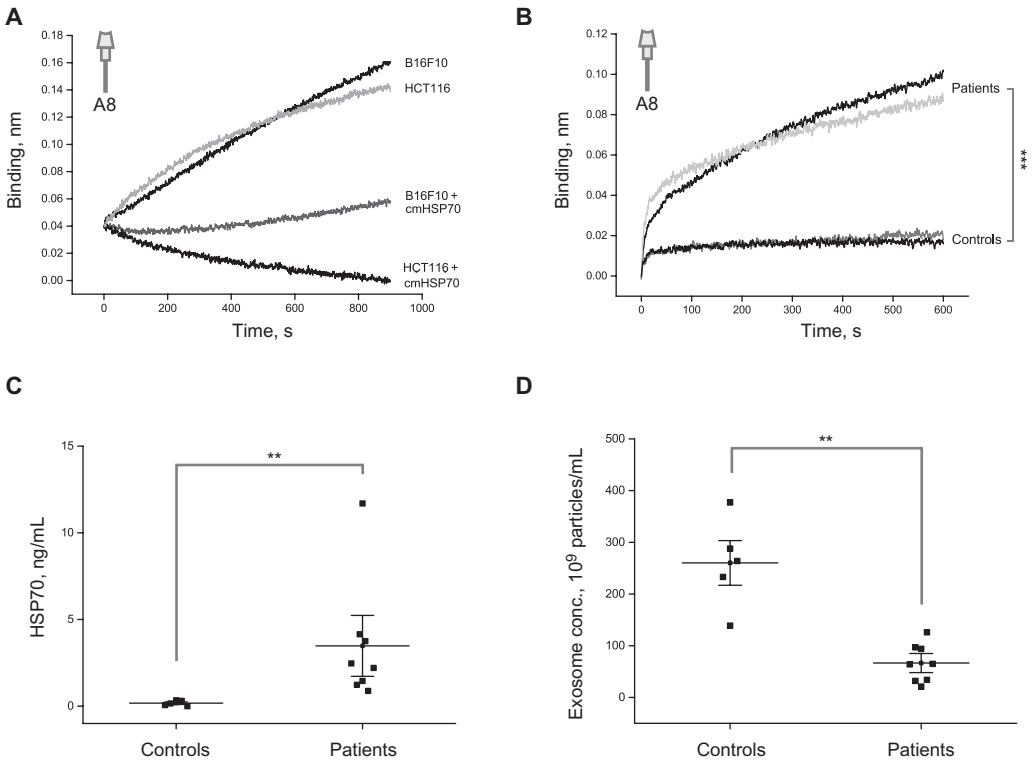

Figure 1. A8 peptide aptamer: a tool to detect exosomes expressing HSP70 in their membranes in cancer samples. **A)** The binding of exosomes (nm), derived from B16F10 or HCT116 cell lines to immobilized biotinylated A8 was determined by biolayer interferometry. Where indicated, cmHSP70 was also added. **B)** Association curves (nm) of HSP70 exosomes in urine samples of patients with breast (n = 3) or pulmonary (n = 3) cancer or healthy individuals (controls, n = 2) with biotinylated A8 immobilized on streptavidin sensor tips. Binding curves represent mean signal of triplicate measurements for each sample. Mann-Whitney: ***$P < .001$. **C)** Exosomes expressing HSP70 were determined by a customized enzyme-linked immunosorbent assay in urine samples from healthy individuals (n = 5) and cancer patients (breast, pulmonary and ovary, n = 8). Data are means and standard deviations of the nanovesicle concentrations ($P = .004$). **D)** Nanoparticle tracking analysis (NTA) to quantify total number of exosomes in the urine samples described above. Samples were diluted in PBS and analyzed using a NanoSight LM10 instrument. Data points are total numbers of exosomes (10^9/mL). **Error bars** represent standard deviations, Mann-Whitney: **$P = .0016$. All statistical tests were two-sided.

to 1.8 μM). A8 also blocked, in a dose-dependent manner, HSP70 chaperone activity as measured by a luciferase refolding assay. For instance, for a three-fold increase in the concentration of A8, we obtain a four-fold reduction in HSP70 chaperon activity ($P = .006$) (Figure 3B).

To further characterize these associations, we next immobilized A8 or TLR2 on the surface of the biosensor and determined their affinity constant (K_D) for HSP70. The K_D of HSP70 for A8 and TLR2 was 2.2 nM and 33 nM, respectively (Figure 3, C and D), indicating that HSP70 displays a greater affinity for A8 than for TLR2. This could explain why A8 prevents the interaction between HSP70 and TLR2.

A8 Blocks the Ability of Tumor-Derived Exosomes to Activate MDSCs

The TLR2-dependent activation of MDSC by exosomes involves IL-6 release that triggers the activation of its receptor and the phosphorylation of STAT3 (27,28). Therefore, we evaluated the ability of A8 to prevent the activation of MDSCs by exosomes by determining IL-6 secretion and STAT3 phosphorylation status.

MSC2s were incubated in the presence or absence of TDEs (isolated from B16F10 cells) and/or A8. Supernatants were harvested and secreted IL-6 quantified by ELISA. As expected, we found that TDEs stimulate the secretion of IL-6 induced by MSC2s. Importantly, this IL-6 production was dose-dependently abrogated by A8 (ie, 81 pg/mL ± 19 vs 28 pg/mL ± 0.7 and 19 ± 1, $P = .04$ for a concentration of A8 of 8 μM and 16 μM, respectively) (Figure 4A). A8 provoked a similar blockage of IL-6 release induced by TDEs when, instead of MSC2, we used primary MDSC isolated from the spleen of mice (109.4 pg/mL ± 14 vs 5.26 pg/mL ± 3.9 in the presence of 16 μM A8, $P = .012$) (Figure 4B).

Then, we studied STAT3 phosphorylation kinetics by western blot in MSC2s induced by TDEs isolated from the supernatant of the four different cancer cell lines (B16F10, CT26, HCT116, or SW480) with or without A8. In the absence of TDEs, hardly any phosphorylation of STAT3 in MSC2s was observed, indicating little or no activation of STAT3 at basal level (Figure 4C), and that A8 does not have a direct effect (Supplementary Figure 4A, available online). In contrast, in the presence of TDE STAT3 phosphorylation was induced (Figure 4C). The addition of A8 in the culture medium inhibited the ability of TDEs to phosphorylate STAT3 in MSC2s. This effect was reproducible because this inhibitory effect was observed with exosomes isolated from four different cancer cells (Figure 4C). Further, a similar inhibitory effect of STAT3 phosphorylation by A8 was observed in primary MDSCs (Figure 4D). To confirm the role of A8 blocking the activation of MDSCs by TDEs, we analyzed other markers of MDSC activity, ie, IL-10 release and MDSCs' ability to induce the release of IFNγ by naive T-cells. As shown in Figure 4, E and F, A8 blocked the ability of TDEs to induce IL-10 release on MDSC (108 pg/mL ± 11 vs 56 pg/mL ± 6.6, $P = .049$) and was able to rescue T-cell activation (IFNγ release: 1657 pg/mL ± 45 vs 115 pg/mL ± 54, $P = .008$).

To further prove that the inhibitory effect of A8 on MSC2 activation was because of its direct interaction with the extracellular domain of HSP70 at the exosomes surface, we tested the effect of A17, another peptide aptamer. We previously demonstrated that A17 binds to the ATP-binding domain of HSP70,

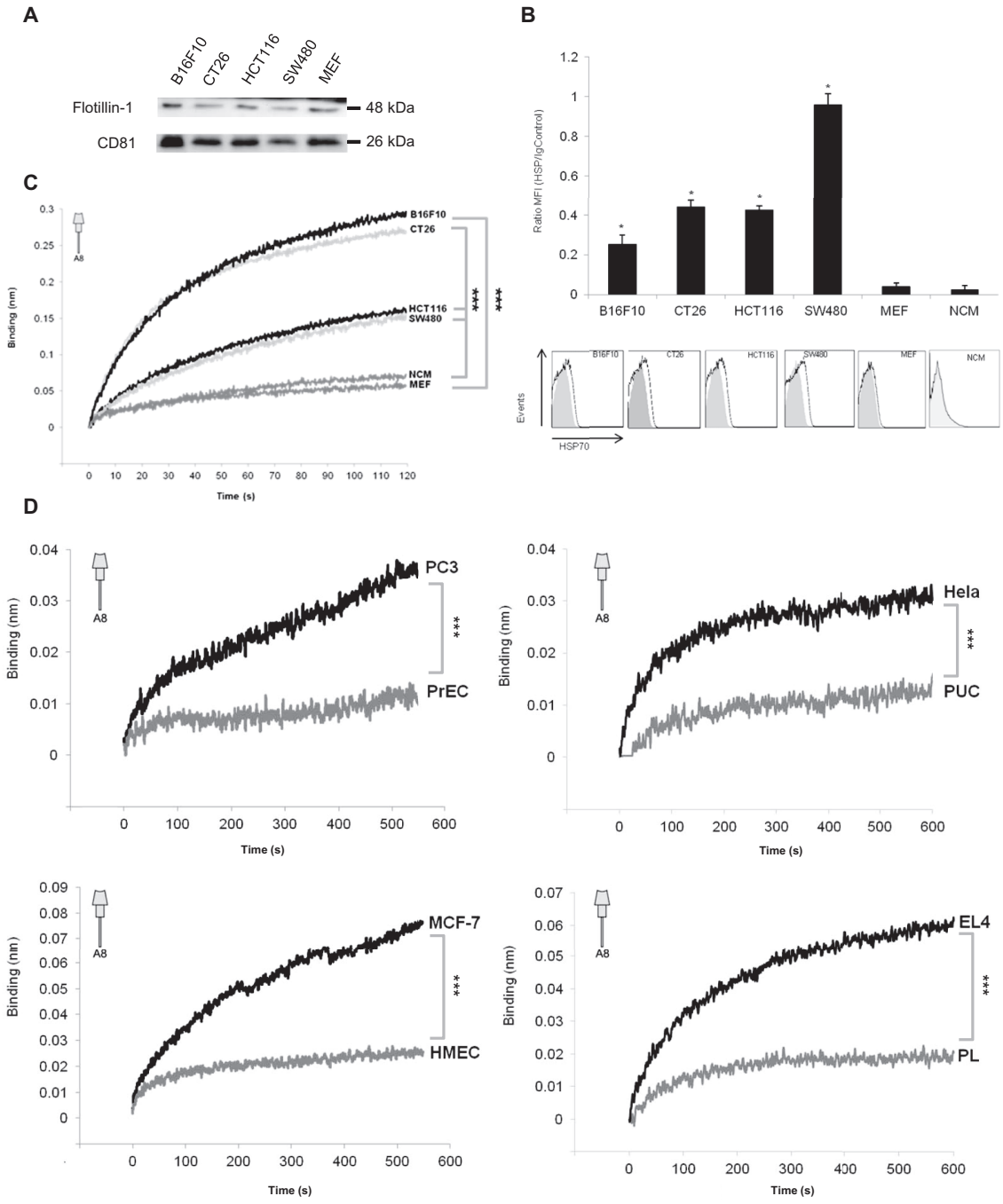

Figure 2. Exosomes derived from human and mouse cancer cell lines express HSP70 on their membranes. **A)** A representative western blot of Flotillin-1 and CD81 expression in exosomes isolated from mouse embryonic fibroblasts (MEFs), B16F10, CT26, HCT116, and SW480 cells' supernatants (n = 3). **B)** Membrane-bound HSP70 in exosomes isolated from B16F10, CT26, HCT116, SW480, MEF, and normal colon mucosa (NCM) was determined by flow cytometry. Data represent means ± SD of the ratio of MFI cmHSP70/ MFI Ig control (n = 3). Two-sided *t* test: *P < .05. **Lower panels** are representative FACS histograms. **C)** Binding of exosomes (nm), derived from MEF, NCM, B16F10, CT26, HCT116, and SW480 cells to immobilized biotinylated A8 was determined by biolayer interferometry. MEF and NCM that showed little binding are considered negative controls for HSP70 exosomes. Binding curves represent mean signal of triplicate measurements. Mann-Whitney: ***P < .001. **D)** Binding of exosomes (nm), derived from PC3, HeLa, MCF-7, and EL4 cancer cells, to immobilized biotinylated A8 was determined by biolayer interferometry. Each cancer cell was compared with the following normal counterparts: prostate epithelial cells (PrEC), primary uterine cells (PUC), human mammary epithelial cells (HMECs), and primary lymphocytes (PLs). Mann-Whitney: ***P < .001. All statistical tests were two-sided. Binding curves represent mean signal of triplicate measurements.

which is located in the intracellular N-terminal region of membrane-bound HSP70 (23). As shown in Supplementary Figure 4B (available online), A17, in contrast to A8, did not interfere with the ability of tumor-derived exosomes to induce STAT3 phosphorylation in MSC2s.

We also checked by FACS whether A8, when incubated with tumor-derived exosomes, could affect the survival of MSC2s. As shown in Supplementary Figure 4C (available online), A8 alone or together with tumor-derived exosomes, did not induce any substantial cell death.

Altogether, these results demonstrate that A8, by its interaction with the extracellular domain of HSP70 in the tumor-derived exosomes, blocks their ability to induce the activation of MDSCs through the STAT3-signaling pathway. Because it has

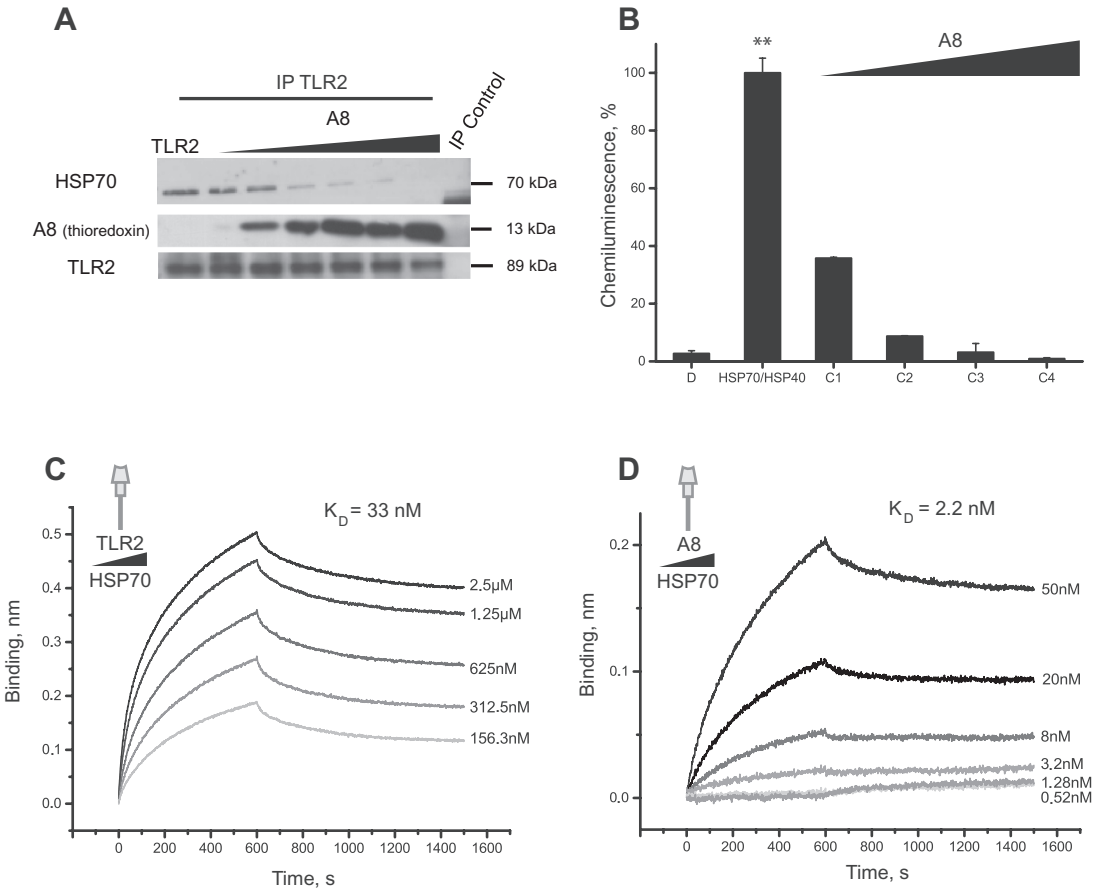

Figure 3. A8 blocks HSP70/TLR2 association. **A)** Immunoprecipitation of toll-like receptor 2 (TLR2) in the presence of increasing concentrations of A8 (from 0.3 μM to 1.8 μM) was followed by HSP70 immunoblotting. IP control: nonrelevant IgG antibody. In this experiment, thioredoxin antibody is used to detect A8. **B)** Denatured luciferase (named D) was incubated in the absence or presence of human HSP70, and when indicated increasing concentrations of A8 (C1 = 5 μM, C2 = 15 μM, C3 = 25 μM, and C4 = 50 μM) for one hour at 25°C. Following incubation, the luciferase substrate D-luciferin was added and within 10 minutes the total light units emitted were collected for 10 seconds at 560 nm using a Wallac (Victor 3) spectrophotometer. Data represent mean % ± SD of three independent experiments. Two-sided *t* test: **P = .006. **C)** Biolayer interferometry to determine association and dissociation curves of HSP70 (concentration range from 2.5 μM to 156.3 nM) with biotinylated TLR2 immobilized on streptavidin sensor tips. **D)** Association and dissociation curves of HSP70 (concentration range from 50 nM to 0.52 nM) with biotinylated A8 immobilized on streptavidin sensor tips. Curves in **(C)** and **(D)** represent mean signal of triplicate measurements for each concentration.

been reported that MDSC activation results in a consequent IL-6-dependent proliferation loop (29), we also checked the effect of A8 in MDSC proliferation. As shown in Supplementary Figure 5 (available online), A8 blocked TDE-induced proliferation both in cultures of MSC2s and primary MDSCs.

Tumor-Bearing Mice Treated With A8 Develop an Anticancer Immune Response Involving MDSCs

To study the effect of A8 in vivo, we used two rodent cancer models: melanoma B16F10 and lymphoma EL4 tumors developed in C57BL/6 mice. We performed subcutaneous injection of cells or media as a control at day 0, and when tumor size reached about 0.9 mm^3 mice were treated i.p. with a control peptide aptamer (A0) or A8 every two days until the end of the experiment. When indicated, half of the mice received i.p. a single dose of cisplatin (5 mg/kg) or 5-fluorourcil (5FU, 25 mg/kg) for the B16F10 or EL4 models, respectively. At day 12 (B16F10) or 10 (EL4), we analyzed the percentage of MDSCs present in mice spleens (n = 6 mice per group) (Figure 5A for the B16F10 model and Figure 5B for the EL4 model). In agreement with the literature (30), we found 2.5 % ± 0.9 of MDSC in the spleen of mice with no tumors (controls, n = 6 per group), whereas in tumor-bearing mice (and control-treated with an A0 aptamer that does not bind to HSP70) (23) we observed a four- to five-fold increase in the percentage of MDSC (compare 2.5 % ± 0.9 vs 12.9 % ± 1.2; Figure 5A; or vs 14.3 ± 1.7; Figure 5B; P = .02). Importantly, this increase was strongly decreased in tumor-bearing mice treated by A8, where we obtained values of 6 ± 0.7 (Figure 5A) or 5.3 % ± 0.3 (Figure 5B, P = .02, n = 6 for each group). In tumor-bearing mice treated with cisplatin or 5FU alone, the percentage of MDSCs was 9 % ± 1 and 4.75 % ± 1.2, respectively, for the B16F10 an EL4 models, whereas in the spleen of tumor-bearing mice treated with both A8 and cisplatin or A8 and 5FU only barely 2.7 % ± 0.8 and 1.83 % ± 0.9 of MDSCs were found. Remarkably, these percentages were similar to that found in mice bearing no tumors. A8 not only decreased the number of MDSCs after cisplatin treatment but also, as expected, affected their activity as determined by phosphorylated STAT3 (Figure 5A).

In the two models, the decrease in MDSC induced by A8 was associated with tumor regression (eg, in the CDDP- and 5FU-treated mice, n = 6 mice/group, the mean tumor volume diminished from 1950 mm^3 ± 620 to 523 mm^3 ± 70, P = .049, for the B16F10 model; Figure 5C; and from 1303 mm^3 ± 93 to 81 mm^3 ± 39, P = .0048, for the EL4 model; Figure 5D) and with intratumor infiltration of immune cells, notably T cells ($CD3^+$), dendritic cells ($CD11c^+$), and macrophages ($F4/80^+$) (Figure 5E; Supplementary Figure 6, available online). Interestingly, macrophages that

ARTICLE

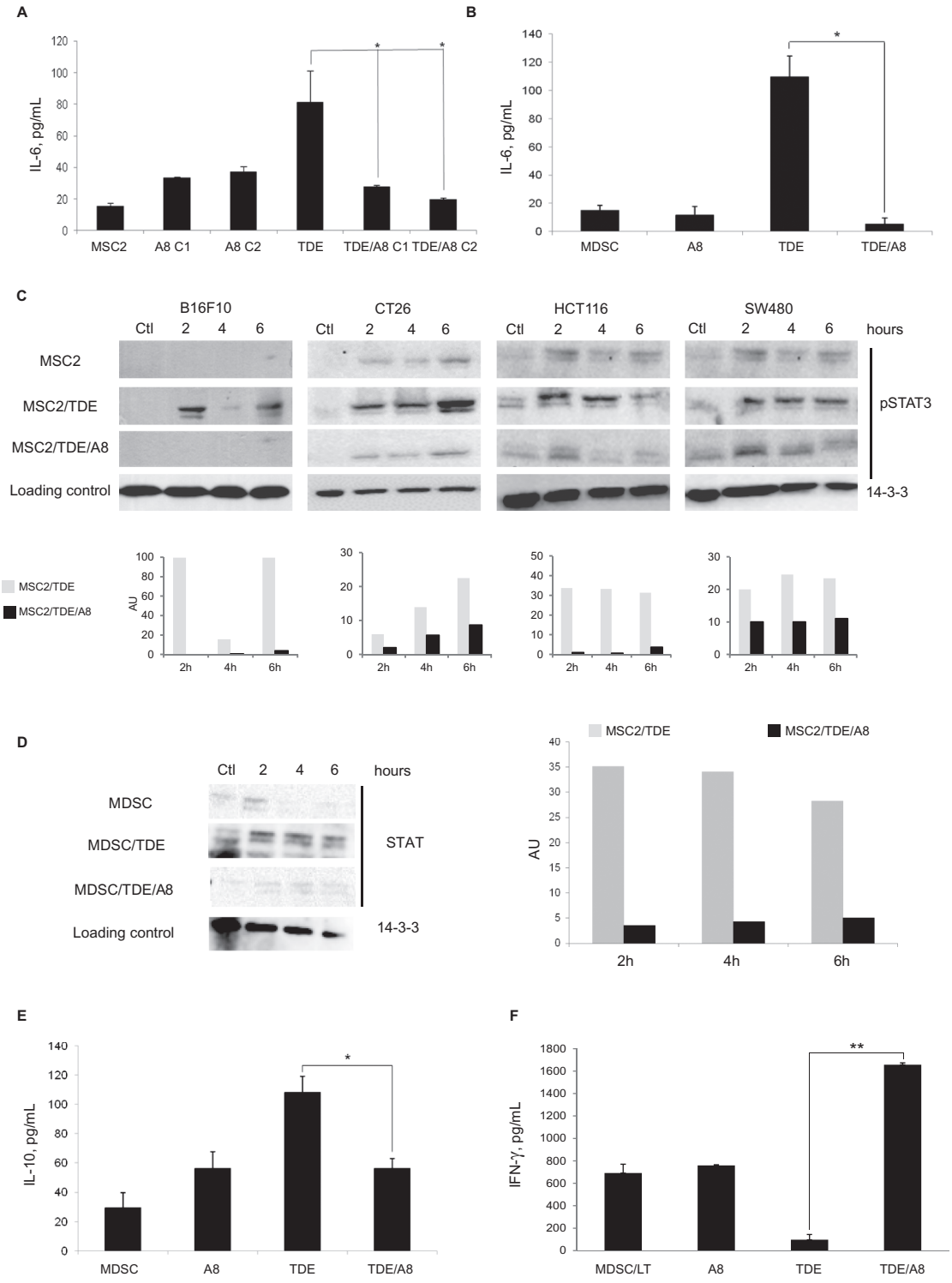

Figure 4. A8 blocks the activation of MSC2 and primary MDSC cells. **A)** IL-6 concentration was determined by enzyme-linked immunosorbent assay (ELISA) in the supernatant of myeloid suppressor cell 2 (MSC2) incubated or not for 24 hours with exosomes (from B16F10) in the absence or presence of A8 (A8 C1: 8 μM, A8 C2: 16 μM). Two-sided *t* test: *P = .04, n = 3). **B)** IL-6 concentration was determined by ELISA in the supernatant of myeloid-derived suppressor cells (MDSCs) incubated or not for 24 hours with exosomes (from B16F10) in the absence or presence of A8 (16 μM). Data are mean pg/mL ± SD. Two-sided *t* test: *P = .012, (n = 3). **C)** A representative image of a western blot (and quantification of the amount of pSTAT3 by densitometry analysis, relative absorbance units) showing the kinetics of STAT3 phosphorylation in MSC2 incubated or not with exosomes isolated from B16F10, CT26, HCT116, or SW480 cells together with a A0 peptide aptamer control (MSC2/TDE) or A8 (MSC2/TDE/A8). **D) Left panel**, a representative image of a western blot showing STAT3 phosphorylation in MDSC incubated or not with exosomes isolated from B16F10 cells together with a peptide control (MDSC/TDE) or A8 (MDSC/TDE/A8). **Right panel**, quantification of the amount of pSTAT3 by densitometry analysis, relative absorbance units. **E)** IL-10 concentration was determined by ELISA in the supernatant of MDSCs incubated or not for 24 hours with exosomes (from B16F10) in the absence or presence of A8 (16 μM), P = .049, n = 3). **F)** IFNɣ concentration was determined by ELISA in the supernatant of T lymphocytes cocultured with MDSC cells, incubated or not for five days with exosomes (from B16F10) in the absence or presence of A8 (16 μM). Data are mean pg/mL ± SD. Two-sided *t* test: **P = .008 (n = 3).

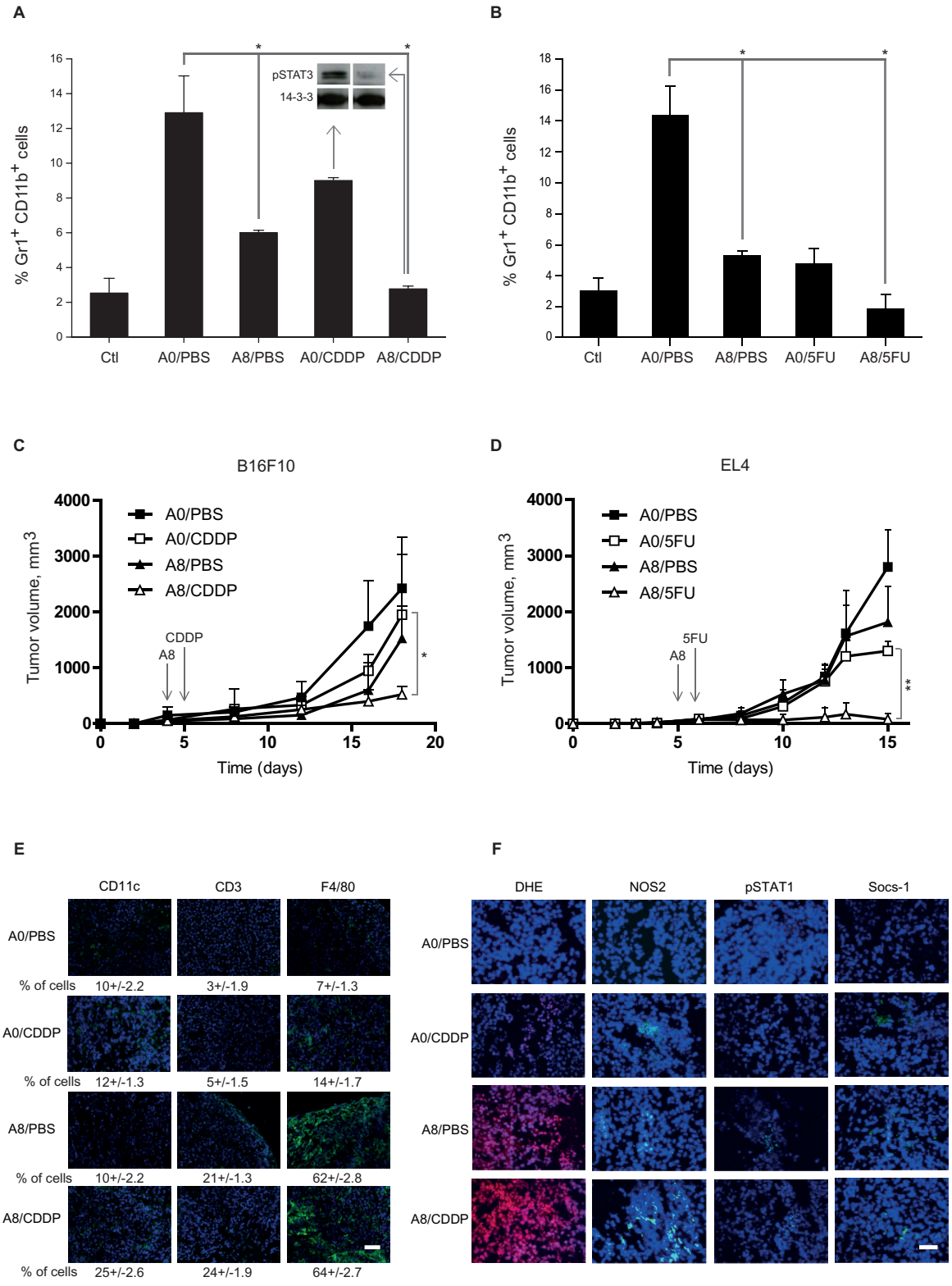

Figure 5. A8 antitumor effect in mice is associated with an increased antitumor immune response. Mice were s.c. injected with B16F10 cells ($5x10^4$) or with EL4 cells ($7x10^5$). On day 4–5, mice were treated every two days until the end of the experiment, with either A0 (control aptamer) or A8 (3 mg/kg, i.p. injection). On day 5–6, half the mice were i.p. treated with a single dose of cisplatin (CDDP, 5 mg/kg) for the B16F10 model or 5-fluorouracil (5FU, 25 mg/kg) for the EL4 model. **A-B)** At day 12 (B16F10) or 10 (EL4), the percentage of MDSC ($Gr1^+$ $CD11b^+$) cells in the spleen collected from the different groups of mice was analyzed by flow cytometry (6 mice per group). As a negative control (Ctl), we used mice with no tumors. Insert shows a representative immunoblot of pSTAT3 in the MDSC isolated from the spleen of A0/CDDP- and A8/CDDP-treated mice. 14-3-3 was used as a loading control. Data are mean % ± SD. Two-sided *t* test: *P = .02. **C-D)** Tumor size was measured every two days (6 mice per group; one representative experiment out of 3 performed is shown). The **open symbols** represent mice treated with cisplatin **(C)** or 5FU **(D)**. Data are mean ± SD. Two-sided *t* test: *P = .049, **P = .0048. **E)** B16F10 tumor sections were performed 14 days after injection of A8. Dendritic cells, T cells, and macrophages were labeled using the monoclonal antibodies CD11c (1/50 dilution), CD3 (1/50), and F4/80 (1/100), respectively. DAPI overlay images are shown. A representative image is shown (n = 6 per group). Labeled cells were counted from 300 cells chosen randomly in different microscopic fields. **Scale bar** = 30 μm. **F)** Macrophages M1 markers in the tumor section described above were determined by DHE/DAPI, SOCS1/DAPI (1/200 dilution, polyclonal), p-STAT1/DAPI, and NOS2/DAPI (1/200 dilution, polyclonal) staining. One representative image is shown (n = 6 per group). **Scale bar** = 30 μm.

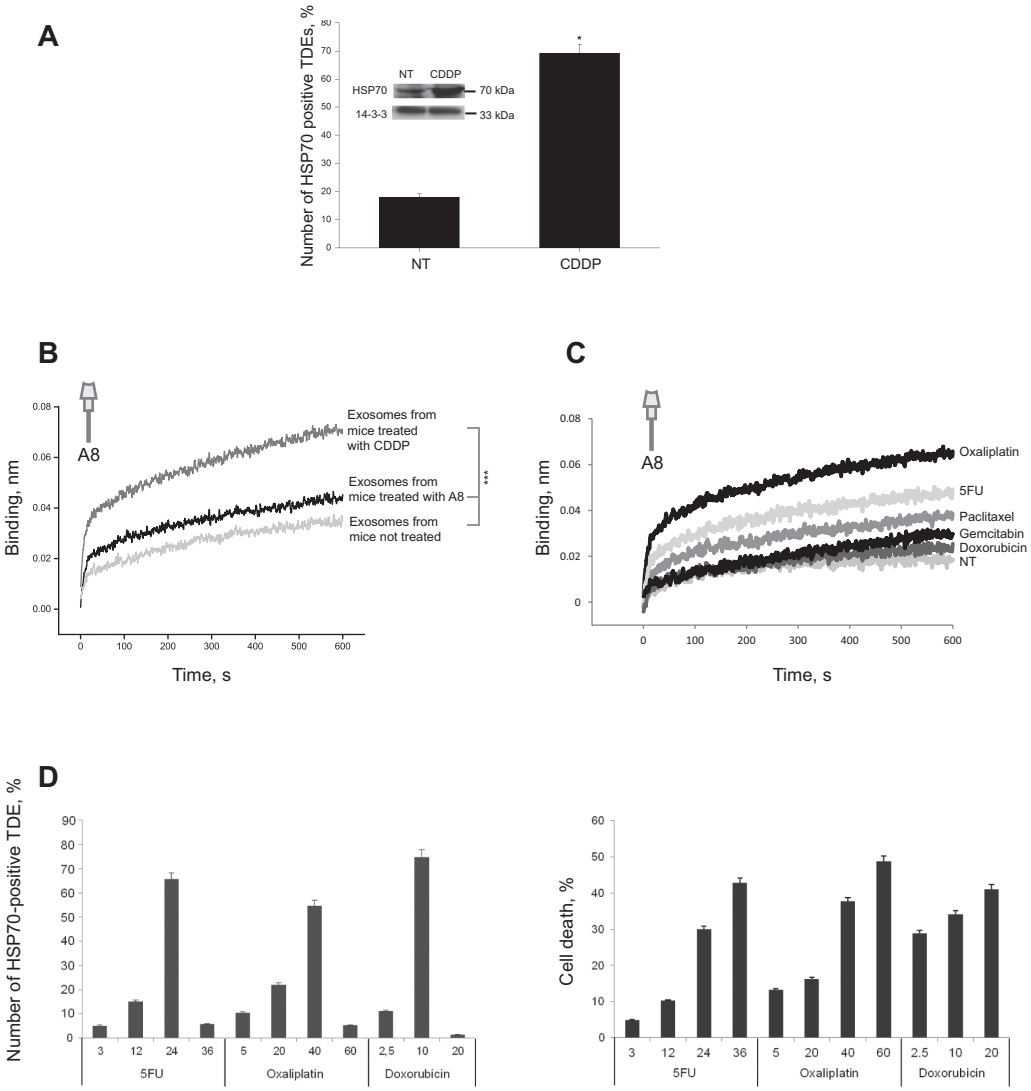

Figure 6. Effect of chemotherapy drugs on HSP70-exosome release. **A)** HSP70 exosomes isolated from B16F10 cells treated or not with cisplatin (CDDP, 25 μM) were determined by flow cytometry, (n = 3). Data are mean % ± SD. Two-sided *t* test: *P = .04. **B)** Association curves of HSP70 exosomes present in sera of tumor-bearing mice treated or not with A8 or cisplatin (5 mg/kg). For the BLI, biotinylated A8 was immobilized on streptavidin sensor tips, n = 3 (for each curve, the blood of 6 mice per group was pooled). Binding curves represent mean signal of triplicate measurements. Two-sided *t* test: ***P < .001. **C)** Association curves of HSP70 exosomes isolated from the supernatant of HCT116 cells treated or not with oxaliplatin (5 μM), 5FU (3 μM), paclitaxel (50 nM), gemcitabin (10 μM), and doxorubicin (2.5 mM). For the BLI, biotinylated A8 was immobilized on streptavidin sensor tips. Binding curves represent mean signal of triplicate measurements. **D)** HCT116 cells were treated with 5FU (3, 12, 24, and 36 μM) or oxaliplatin (5, 20, 40, and 60 μM), or doxorubicin (2.5, 10, and 20 μM) for 48 hours. **Left panel**, concentration of HSP70 exosomes released was measured by flow cytometry. **Right panel**, measured apoptosis of HCT116 (7AAD and FITC-Annexin V). Data are means percentages ± SD of three experiments.

abundantly infiltrated the tumor in A8-treated mice were skewed toward the cytotoxic phenotype as demonstrated by DHE, NOS2, pSTAT1, and Socs1 markers (Figure 5F).

We then determined whether cisplatin or 5FU increased the amount of HSP70 exosomes, which could explain why their combination with A8 decreased MDSCs and increased the drugs' antitumor properties. We isolated total exosomes from both cultured B16F10 (Figure 6A) and blood of tumor-bearing mice (Figure 6B) by ultracentrifugation and quantified HSP70 exosomes by FACS and BLI, respectively. We found that the amount of HSP70 exosomes released by B16F10 cells strongly increased after cisplatin treatment (19 % ± 2.9 vs 69±7, P = .04) (Figure 6A) and that the amount of HSP70 exosomes in the blood was much higher in cisplatin-treated mice (mean signal of 0.02 nm ± 0.01 vs 0.06 nm ± 0.01, P < .001) (Figure 6B). We tested whether this ability to increase the number of HSP70 exosomes was specific to cisplatin or could be extended to other anticancer drugs. As shown in Figure 6C, all drugs tested at toxic equivalent concentrations, to a greater (oxaliplatin, 5FU) or lesser (doxorubicin) extent, induce an increase in the amount of HSP70 exosomes. A dose-response release of HSP70 exosomes for cisplatin, 5FU, and doxorubicin is shown in Figure 6D. We observed for the three drugs that the amounts of HSP70 exosomes released increased with drug concentration, but only for concentrations inducing a relatively low amount of cell death. At higher doses inducing more than 40% cell death, the number of exosomes drastically decreased, suggesting that increased HSP70 exosome amount is not just because of cell death and release. For example, for 5FU concentrations of 3,12, 24, and 36 μM inducing a percentage of cell death of 4.8, 10.2, 30, and 43, respectively, we obtained a percentage of HSP70 exosomes released of 5.1, 12, 65, and only 6.6, respectively (Figure 6D, left and right panels).

Discussion

In this study, we demonstrated that the peptide aptamer A8 tightly binds to extracellular membrane-bound HSP70 present in TDEs and that this association blocks the ability of exosomes to activate

MDSCs. We show in vivo the utility of associating A8 with a chemotherapeutic drug (cisplatin, 5-fluorouracil) in order to restore an efficient antitumoral immune response. Finally, we showed proof of principle that A8 can be used to quantify TDEs in human samples. The advantage of using A8 over antibodies targeting extracellular HSP70 such as cmHSP70 is that peptide aptamers are stable, soluble, easy to produce, and small (~11kDa) (25).

As cancer cells accumulate mutations, violate physiological laws, and acquire sets of hallmarks (31), they require a constitutively high level of chaperones like HSP70 for their survival/maintenance. Because only 10% of the total amount of intracellular HSP70 is expressed at the cytoplasmic membrane, this most likely explains why exosomes from normal cells are devoid of membrane-bound HSP70. Here, we have used a peptide aptamer, A8, targeting the extracellular domain of HSP70 on exosomes, blocking HSP70 association with the MDSC receptor TLR2 and thus MDSC activation. A8 also blocked MDSC proliferation, probably because of its ability to inhibit IL-6 production and pSTAT3, which can affect the expression of genes such as cyclin D, Mcl1, or Myc, reported to be involved in cell growth (32). A8-induced reduction in the number of MDSCs in the spleens of tumor-bearing mice, which was particularly strong after cisplatin or 5FU treatment, could not be explained by a possible repositioning of MDSC, at least from the spleen toward the tumors, because tumor infiltration with MDSCs was very scarce in all mice, with no statistically significant differences among the groups (data not shown).

A8, by interfering with the immune suppressive functions of TDEs, may improve the efficacy of anticancer drugs. Indeed, we demonstrated that cisplatin or 5FU combined with A8 decreased tumor growth and favored the development of an anticancer immune response characterized notably by an important infiltration of cytotoxic M1-like macrophages. Although T-cells are the direct target of MDSCs, this macrophage infiltration can be explained by the reported cross-talk existing between MDSC/T-cells and macrophages (33). Indeed, T-cells are the primary immune cells responsible for the A8 antitumor effect as demonstrated by the fact that: 1) in nude mice, the A8 antitumor effect is completely abolished (23) and 2) as shown in this work, the A8 effect directly involves MDSCs, whose main direct targets are T-cells. To determine which subset of T-cells is responsible for the A8 effect, we immunodepleted CD4+ or CD8+ cells by repetitive i.p. injection with specific neutralizing antibodies. Our results clearly show that whereas CD8 depletion inhibits A8 antitumor effect, CD4 depletion does not seem to have any notable effect (Supplementary Figure 7, available online).

Interestingly, A8 biodistribution experiments, after systemic administration, demonstrate that the peptide localizes mainly in the tumor area (34), likely because of the abundant expression of HSP70 in tumors. Considering the general role of HSP70 in different cancers and its induction by a large panel of anticancer agents, the anticancer immune approach proposed in this work involving inhibition of HSP70 exosomes might be extended to different cancer types with their respective chemotherapeutic setups. It is worth noting that neither our studies nor those done for the biodistribution of A8 indicated any evident toxicity in the mouse models, notably cardiac or hepatic.

Besides the rationale for a combination therapy, our results in human samples suggest that HSP70 exosomes could be used as a cancer biomarker (Supplementary Figure 8, available online). The main advantage to quantifying tumor-derived exosomes compared with circulating tumor cells (CTCs) is that exosomes are found in large amounts compared with CTCs and that exosomes can be quantified both in blood and urine, as demonstrated here.

The main limitation of this study is the small number of patients analyzed. To confirm our results, we have just started a three-year prospective study with the anticancer Centre Georges-François Leclerc (Dijon, France) that will include 60 breast, ovary, and lung cancer patients and 20 healthy voluntary donors. In this prospective study and follow-up clinical trial, we will determine whether the presence of HSP70 exosomes is predictive of patient response to chemotherapy and whether its detection precedes that of CTCs (CellSearch) and the appearance of metastases (determined by medical imaging).

Funding

This work was supported by the Institut National du Cancer, European Commission's Seventh Framework Programme (SPEDOC 248835) (C. Garrido), the Agence Nationale de la Recherche, the Institut National du Cancer, and the Conseil Regional de Bourgogne (C. Garrido). H. Mjahed acknowledges a fellowship from SPEDOC, J. Gobbo from the "Ligue contre le Cancer," and G. Marcion from the "Ministère de l'Enseignement Supérieur de la recherche." Carmen Garrido's team is labeled by La Ligue Nationale contre le Cancer, the "Association pour la Recherche sur le Cancer" (ARC). This work was supported by a French Government grant managed by the French National Research Agency under the program "Investissements d'Avenir" with reference ANR-11-LABX-0021 (LabEX LipSTIC). We thank the FEDER for their financial support.

Notes

We thank G. Multhoff (Technische Universitat Munchen, Munich, Germany) for helpful discussions.

The authors have no conflicts of interest to declare.

References

1. Liu Y, Wang L, Predina J, et al. Inhibition of p300 impairs Foxp3+ T regulatory cell function and promotes antitumor immunity. *Nat Med*. 2013;19(9):1173–1177.
2. Chhabra A, Mukherji B. Death Receptor-Independent Activation-Induced Cell Death in Human Melanoma Antigen-Specific MHC Class I-Restricted TCR-Engineered CD4 T Cells. *J Immunol*. 2013;191(6):3471–3477.
3. Galdiero MR, Bonavita E, Barajon I, Garlanda C, Mantovani A, Jaillon S. Tumor associated macrophages and neutrophils in cancer. *Immunobiology*. 2013;218(11):1402–1410.
4. Khaled YS, Ammori BJ, Elkord E. Myeloid-derived suppressor cells in cancer: recent progress and prospects. *Immunol Cell Biol*. 2013;91(8):493–502.
5. Nagaraj S, Collazo M, Corzo CA, et al. Regulatory myeloid suppressor cells in health and disease. *Cancer Res*. 2009;69(19):7503–7506.
6. Serafini P, Borrello I, Bronte V. Myeloid suppressor cells in cancer: recruitment, phenotype, properties, and mechanisms of immune suppression. *Semin Cancer Biol*. 2006;16(1):53–65.
7. Serafini P, De Santo C, Marigo I, et al. Derangement of immune responses by myeloid suppressor cells. *Cancer Immunol Immunother*. 2004;53(2):64–72.
8. Bobrie A, Théry C. Exosomes and communication between tumours and the immune system: are all exosomes equal? *Biochem Soc Trans*. 2013;41(1):263–267.
9. Ostrowski M, Carmo NB, Krumeich S, et al. Rab27a and Rab27b control different steps of the exosome secretion pathway. *Nat Cell Biol*. 2010;12(1):19–30; sup pp 1–13.
10. McLellan AD. Exosome release by primary B cells. *Crit Rev Immunol*. 2009;29(3):203–217.
11. Knight AM. Regulated release of B cell-derived exosomes: do differences in exosome release provide insight into different APC function for B cells and DC? *Eur J Immunol*. 2008;38(5):1186–1189.
12. Kapsogeorgou EK, Abu-Helu RF, Moutsopoulos HM, Manoussakis MN. Salivary gland epithelial cell exosomes: A source of autoantigenic ribonucleoproteins. *Arthritis Rheum*. 2005;52(5):1517–1521.
13. Théry C, Ostrowski M, Segura E. Membrane vesicles as conveyors of immune responses. *Nat Rev Immunol*. 2009;9(8):581–593.
14. Valadi H, Ekström K, Bossios A, Sjöstrand M, Lee JJ, Lötvall JO. Exosome-mediated transfer of mRNAs and microRNAs is a novel mechanism of genetic exchange between cells. *Nat Cell Biol*. 2007;9(6):654–659.

ARTICLE

15. Peinado H, Alečković M, Lavotshkin S, et al. Melanoma exosomes educate bone marrow progenitor cells toward a pro-metastatic phenotype through MET. *Nat Med*. 2012;18(6):883–891.
16. Bobrie A, Colombo M, Raposo G, Théry C. Exosome secretion: molecular mechanisms and roles in immune responses. *Traffic*. 2011;12(12):1659–1668.
17. Chalmin F, Ladoire S, Mignot G, et al. Membrane-associated Hsp72 from tumor-derived exosomes mediates STAT3-dependent immunosuppressive function of mouse and human myeloid-derived suppressor cells. 2010;120(2):457–471.
18. Balaburski GM, Leu JI-J, Beeharry N, et al. A modified HSP70 inhibitor shows broad activity as an anticancer agent. *Mol Cancer Res*. 2013;11(3):219–229.
19. Lanneau D, Brunet M, Frisan E, Solary E, Fontenay M, Garrido C. Heat shock proteins: essential proteins for apoptosis regulation. *J Cell Mol Med*. 2008;12(3):743–761.
20. Jego G, Hazoumé A, Seigneuric R, Garrido C. Targeting heat shock proteins in cancer. *Cancer Lett*. 2013;332(2):275–285.
21. Multhoff G. Heat shock protein 70 (Hsp70): Membrane location, export and immunological relevance. *Methods*. 2007;43:229–237.
22. Stangl S, Gehrmann M, Riegger J, et al. Targeting membrane heat-shock protein 70 (Hsp70) on tumors by cmHsp70.1 antibody. *Proc Natl Acad Sci U S A*. 2011;108(2):733–738.
23. Rérole A-L, Gobbo J, De Thonel A, et al. Peptides and aptamers targeting HSP70: a novel approach for anticancer chemotherapy. *Cancer Res*. 2011;71(2):484–495.
24. Baines IC, Colas P. Peptide aptamers as guides for small-molecule drug discovery. *Drug Discov Today*. 2006;11(7–8):334–341.
25. Seigneuric R, Gobbo J, Colas P, Garrido C. Targeting cancer with peptide aptamers. *Oncotarget*. 2011;2(7):557–561.
26. Stangl S, Themelis G, Friedrich L, et al. Detection of irradiation-induced, membrane heat shock protein 70 (Hsp70) in mouse tumors using Hsp70 Fab fragment. *Radiother Oncol*. 2011;99(3):313–316.
27. Kapanadze T, Gamrekelashvili J, Ma C, et al. Regulation of accumulation and function of myeloid derived suppressor cells in different murine models of hepatocellular carcinoma. *J Hepatol*. 2013;59(5):1007–1013.
28. Xiang X, Liu Y, Zhuang X, et al. TLR2-mediated expansion of MDSCs is dependent on the source of tumor exosomes. *Am J Pathol*. 2010;177(4):1606–1610.
29. Chang Q, Bournazou E, Sansone P, et al. The IL-6/JAK/Stat3 Feed-Forward Loop Drives Tumorigenesis. *Neoplasia*. 2013;15(7):848–862.
30. Kusmartsev S, Cheng F, Yu B, et al. All-trans-retinoic acid eliminates immature myeloid cells from tumor-bearing mice and improves the effect of vaccination. *Cancer Res*. 2003;63(15):4441–4449.
31. Hanahan D, Weinberg RA, Francisco S. The Hallmarks of Cancer Review University of California at San Francisco. *Cell*. 2000;100:57–70.
32. Rébé C, Végran F, Berger H, Ghiringhelli F. A key factor in tumor immunoescape. *JAK-STAT* 2013;2(1):e23010.
33. Sinha P, Clements VK, Bunt SK, Albelda SM, Ostrand-Rosenberg S. Cross-talk between myeloid-derived suppressor cells and macrophages subverts tumor immunity toward a type 2 response. *J Immunol*. 2007;179(2):977–983.
34. Coles DJ, Rolfe BE, Boase NRB, Veedu RN, Thurecht KJ. Aptamer-targeted hyperbranched polymers: towards greater specificity for tumours in vivo. *Chem Commun (Camb)*. 2013;49(37):3836–3838.